Reducing the Uncertainty of Lidar Measurements in Complex Terrain Using a Linear Model Approach

Martin Hofsäß[1],*,[†],[‡] (iD), **Andrew Clifton [2],[‡]** (iD) **and Po Wen Cheng [1],[‡]**

1 Stuttgarter Lehrstuhl für Windenergie, Universität Stuttgart, Allmandring 5b, 70569 Stuttgart, Germany; cheng@ifb.uni-stuttgart.de
2 WindFors—Universität Stuttgart, Allmandring 5b, 70569 Stuttgart, Germany; clifton@windfors.de
* Correspondence: hofsaess@ifb.uni-stuttgart.de; Tel.: +49-(0)711-68568308
† Current address: Allmandring 5b, 70569 Stuttgart, Germany.
‡ These authors contributed equally to this work.

check for updates

Abstract: In complex terrain, ground-based lidar wind speed measurements sometimes show noticeable differences compared to measurements made with in-situ sensors mounted on meteorological masts. These differences are mostly caused by the inhomogeneities of the flow field and the applied reconstruction methods. This study investigates three different methods to optimize the reconstruction algorithm in order to improve the agreement between lidar measurements and data from sensors on meteorological masts. The methods include a typical velocity azimuth display (VAD) method, a leave-one-out cross-validation method, and a linear model which takes into account the gradients of the wind velocity components. In addition, further aspects such as the influence of the half opening angle of the scanning cone and the scan duration are considered. The measurements were carried out with two different lidar systems, that measured simultaneously. The reference was a 100 m high meteorological mast. The measurements took place in complex terrain characterized by a 150 m high escarpment. The results from the individual methods are quantitatively compared with the measurements of the cup anemometer mounted on the meteorological mast by means of the three parameters of a linear regression (slope, offset, R^2) and the width of the 5th–95th quantile. The results show that expanding the half angle of the scanning cone from $20°$ to $55°$ reduces the offset by a factor of 14.9, but reducing the scan duration does not have an observable benefit. The linear method has the lowest uncertainty and the best agreement with the reference data (i.e., lowest offset and scatter) of all of the methods that were investigated.

Keywords: complex terrain; complex flow; lidar; VAD; remote sensing; wind energy

1. Introduction

Doppler wind lidar (light detection and ranging) systems emit laser pulses that are reflected by aerosols in the atmosphere. This backscattered light has a frequency shift (the Doppler effect) due to the movement of the aerosols. The wind speed in direction of the laser beam can be calculated from the frequency shift using the Doppler equation. The alignment of the laser can be described by the azimuth and elevation angle. Ground-based lidar systems can be operated with different operating modes, such as staring, velocity azimuth display (VAD), plan position indicator (PPI) or range height indicator (RHI). The operating modes differ in how the two angles to each other are moved. In PPI mode the elevation angle is fixed and only the azimuth angle is varied over a small sector range. In RHI mode the azimuth angle is fixed and the elevation angle is varied. Both angles are fixed when a lidar operates in a so-called staring mode. The most common mode for commercial wind profilers is the VAD mode. In VAD mode, the azimuth angle is varied over a circle with a fixed elevation angle. The number

of measuring points over the circle are specified by the manufacturer. Also, the backscattered light does not come from a single point but instead along a finite length. This probe length depends on the pulse duration and the measurement technology, for example the use of a pulsed or continuous wave (CW) light source [1]. The CW lidars measure the heights one after the other, while pulsed lidar systems measure several heights simultaneously. It is then possible to estimate a wind vector at one or more points in the lidar scan volume using the wind speed data and azimuth, elevation, and range information and by making assumptions about homogeneity and stationarity. This process is known as wind field reconstruction [1].

Ground-based doppler wind lidar systems have many advantages over wind measurements made with in-situ instruments mounted on meteorological masts (met masts). Commercial ground-based lidar devices can measure at heights up to 300 m, which is above the tip heights of modern wind turbines, while met masts frequently only reach 80–100 m. The lidar can also be reconfigured for different tasks [2], and moved easily so that several locations can be investigated with short measurement campaigns.

Previous comparisons between lidar measurements and measurements made with cup anemometers on met masts show an almost perfect match between the two: [3] estimated a slope of 0.9558 and an offset of 0.1577 m·s^{-1} and a R^2 of 0.9984 in flat terrain and homogeneous flow conditions, while [4] found a slope of 1.004, offset of -0.079 m·s^{-1} and an R^2 of 0.996 based on 10 min averages.

In complex terrain, the correlations between wind speed measurements with single points sensors on met masts and lidar systems show considerable differences. The reason for the large differences are the inhomogeneous flow conditions, which can be caused, for example, by the terrain (momentum-induced turbulence) or by thermal effects (buoyancy-induced turbulence). Further causes can be found in [5]. The magnitude of the differences depends on local conditions:

- Fluctuations in the flow field: Changes in terrain roughness upstream of the measurements cause large variations and changes in wind speed with height lead to uncertainty in the wind speed [6].
- Lidar technology: The weighting function of the lidar signal processing also leads to over- or under estimation of the wind speed.

In this study pulsed ground-based lidar systems were used, which performed modified VAD scans. In a VAD scan, the elevation angle is the half opening angle ϕ of the cone. The lidar devices determine, at selected points, the line-of-sight velocity $v_{los}(\theta, \phi, f_d)$, which is the projection of the wind velocity vector $\vec{v}(x, y, z)$ onto the normal vector $\vec{n}(\theta, \phi)$ of the laser beam (Equation (1), the index indicates the axis direction). The line-of-sight velocity depends on the half opening angle ϕ, the azimuth angle θ and the measuring distance or focal distance f_d. The normal vector is calculated as $\vec{n}(\theta, \phi) = [\cos(\theta)\sin(\phi), \sin(\theta)\sin(\phi), \cos(\phi)] = [n_x, n_y, n_z] = \vec{n}(x, y, z)$ where n_i is the component of the normal vector in $i = x, y, z$ direction. The vector $\vec{n}(\theta, \phi)$ can also be expressed in Cartesian coordinates, which are mainly used in this study. The line-of-sight velocity is given by:

$$v_{los} = u \cdot n_x + v \cdot n_y + w \cdot n_z \tag{1}$$

If v_{los} is measured from multiple azimuthal directions and elevations, the wind velocity components u, v, w can be calculated. If these measurements are made from a single point and encompass a volume of the atmosphere, it must be assumed that $u, v,$ and w apply at all points in the wind field, i.e., that the flow is homogeneous. This leads to errors in the determination of wind speeds in heterogeneous, "complex" flow. Bingöl [7] has shown with a simple mathematical model of a flow over a hill, that the error in the horizontal wind speed can be in the order of magnitude of 10%.

In order to reduce the error during data collection, multi-lidar systems [8–10] can be used. The multi-lidar systems measure simultaneously $v_{los}(x, y, z)$ at the same point. From this system of equations, the wind velocity components can be calculated without assuming the flow is homogeneous. The first simultaneous measurements with several lidar systems were carried out at the *Musketeer Experiment 2007* in flat terrain [8]. Measurements in complex terrain were made during the *Kassel*

Experiment 2014 [9] and during the *NEWA* campaign in Perdigão [11]. However, this measurement configuration is very cost-intensive (greater than 200,000€ per lidar device), which is not affordable for site assessments. Furthermore, a large effort has to be made for a successful operation of the multi-lidar configuration [10].

Another possibility to improve the measurements is to use wind field reconstruction models to better convert v_{los} data into a wind vector or wind field [5,12,13].

Finally, it is possible to use flow modelling to try to reduce differences between lidar measurement and traditional measurements when a campaign has already been completed. These typically focus on the use of commercial Computational Fluid Dynamics (CFD) programs to model flows and "correct" (in reality, "adjust") lidar measurements in complex terrain to better match point measurements from anemometers. Despite a continuing need to validate such tools in complex terrain, a 2015 study [14] concluded that with proper parametrization and flow modelling, flow simulations can be a useful tool in the post-processing of lidar measurements in complex terrain and this is likely to be an important approach in future [2].

In this study, the main focus is on the use of ground-based lidar systems with VAD scan patterns with additional vertical measuring points. This paper introduces several modified measurement strategies and adapted evaluation algorithms to show that it is possible to reduce uncertainties without having to forego the advantages of ground-based lidar systems. The results were also used to explore three questions about the effect of the scan design:

1. Is the length of the trajectory circulation time important in the comparisons with the met mast?
2. Does the half opening-angle ϕ have an influence on the accuracy of the correlations?
3. Is the local resolution of the measurement points important for the result?

Section 2 gives an overview over the measurement campaign, the test site and the methods used for the wind field reconstruction. In Section 3 the results of the comparison between the results of the investigated methods and the reference in-situ measurements are presented. The discussion of the results is in Section 4 and conclusions are presented in Section 5.

2. Materials and Methods

This study uses lidar data obtained during a measurement campaign in complex terrain in Southern Germany. This section provides an overview of the test site, the used measuring systems and the settings and scan patterns. Furthermore, the data preprocessing and data filtering will be discussed. Finally, the wind field reconstruction methods are presented.

2.1. Test Site and Measurement Campaign

The experiment was carried out in south-west Germany on the Swabian Alb. The Swabian Alb extends for around 100 km and can be categorized as a very hilly area consisting of high plateaus surrounded by a pronounced 100–150 m tall wooded escarpment known in the region as the *Albtrauf*. The measurements described here are centred on a 100 m high met mast in relatively flat land less than 1 km from a section of *Albtrauf* (Figure 1).
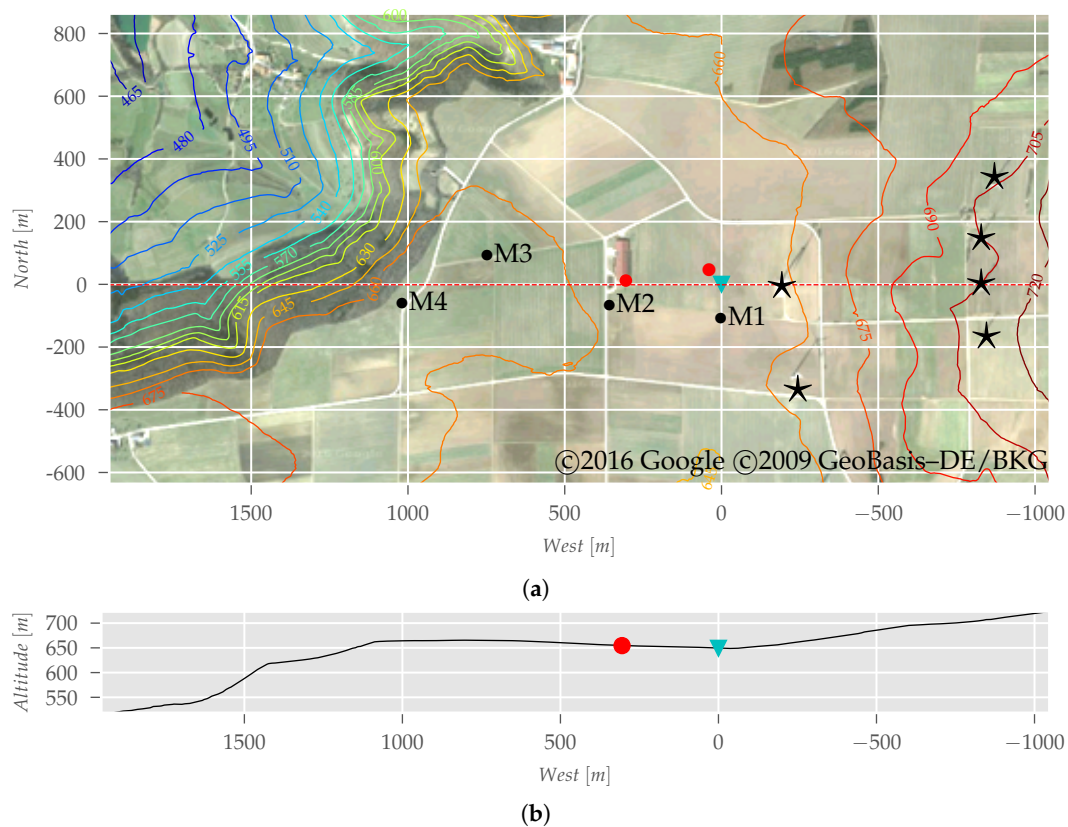
Figure 1. (**a**) The test site topography. An aerial picture (©2016 Google) is overlain with elevation contours (©2009 GeoBasis–DE/BKG, LGL (Geobasisdaten ©LGL Landesamt für Geoinformation und Landentwicklung Baden-Württemberg, Az.: 2851.9-1/19)). The locations of the met mast (▼), lidars (•), wind turbines (⋆), and vertical profiles from [15,16] are also shown. The *Albtrauf* is between the two thicker elevation contours. (**b**) Terrain cross section. The locations of the met mast (▼) and lidars (•) are shown. The experiment site. (**a**) Topography and structures (**b**) Terrain section along red dashed line.

Two wind lidars were installed near the mast. These lidar were the SWE Scanner [17] and a Galion all sky long-range scanning wind lidar. The measurement campaign ran from March 2015 until February 2016. Not all systems were available during the whole measurement period. The SWE Scanner measured from March 2015 to February 2016 and the Galion system measured from March 2015 until June 2015.

Ideally the lidar and met mast would have been co-located or the lidar would been positioned a few 10s of meters upwind of the met mast to avoid wakes. However, this was not possible in this study because the lidars required around 2 kW of power, which could not be supplied directly at the mast's location. Instead the lidars were located at a nearby farm building (visible in Figure 1a), approximately ≈300 m from the met mast.

In a second short measurement period from November 2015 to February 2016 the SWE Scanner was installed at the foot of the met mast guy wires, approximately 48 m from the met mast on a bearing of 330°. During this time the same configuration as in the main measurement period was used, but the number of pulses were lowered from 10,000 to 3000 to reduce the the scanning time. The met mast and both lidar systems were time synchronized with a GPS time signal.

2.1.1. Local Conditions

This site has been the subject of many coordinated studies [16,18–20]. A small remotely-piloted aircraft was used to measure the flow conditions [18]. Detailed Detached-Eddy Simulations (DES) of the flow have been validated using different measurement methods [15,16]. Wind tunnel tests and CFD simulations have also been to model the flow over the site [20].

The wind at this site is mostly from the west to north-west (Figure 2). Around 38% of winds are perpendicular to the *Albtrauf*, and so changes in wind direction of 10° can result in significantly different inflow profiles downwind of the *Albtrauf* [21].
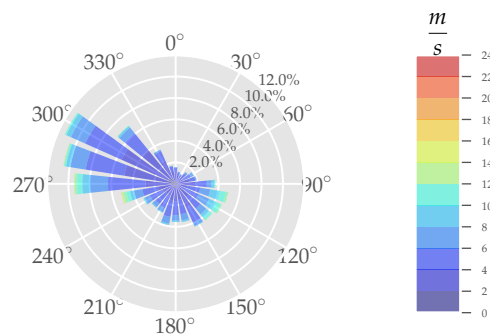

Figure 2. Windrose at the experiment site.

The goal of this study is to compare the data from the met mast and the lidar to assess different measurement and data processing approaches. It is therefore essential that there is minimal external influence on the results, for example as a result of differences in flow between the lidar and tower that might be introduced by the ground cover or the terrain. The impact of these differences can be judged using the International Electrotechnical Committee (IEC) 61400-12-1 Standard (2005, [22]) for power performance testing of wind turbines, which quantifies the potential impact of obstacles as a function of size and distance. At 1400 m south-west of the mast, there is a small forest (not visible in Figure 1), which, according to the Standard, is far away enough that it should not have an influence. East of the met mast, the terrain rises again up to a height of 720 m above sea level. There are also several commercial wind turbines near to the mast which could influence the flow. These obstructions would therefore reduce the free stream sector (according to [22]) from 171° to 341°. However, this large a sector still introduces the chance for flow differences between the devices.

Other studies of this site can be used to understand the podar location and the met mast. The vertical wind profile at the points M1–M4 in Figure 1a was simulated for wind from 295° using CFD that was validated against measurements from an unmanned aerial vehicle [15,16]. Results from the CFD (Figure 3) showed a speed-up of ≈20% at 100 m above ground at M4, closest to the escarpment. At M3 the speed-up factor at 100 m above ground is ≈1.15, while at M1 the speed up effect has disappeared and the vertical profile is fully recovered. From these profiles it can also be seen that the 100-m wind speed at M2 is within 2% of M1, i.e., the mean wind speed difference between M2 (near the lidar) and M1 (near the met mast) is minimal. Based on the results from the CFD study, it was decided to limit the data used to a 70° inflow wind direction sector from 245° to 315°.
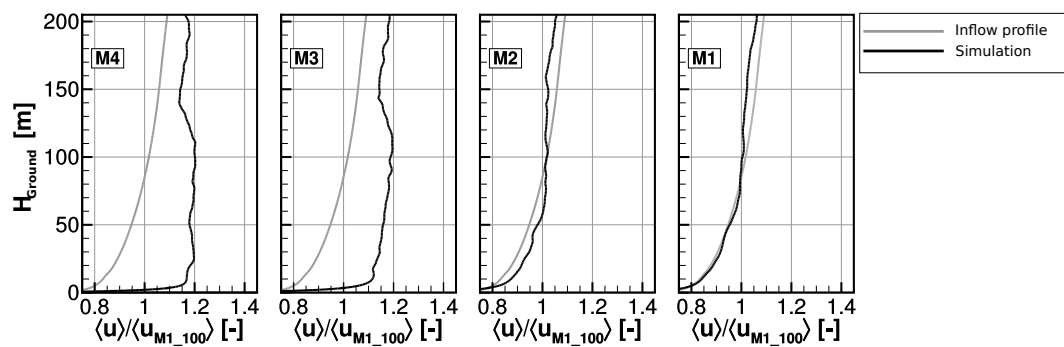
Figure 3. The vertical wind profile near the escarpment and on the plateau. M4 is at the escarpment, M2 is closest to the lidar, and M1 is closest to the met mast (Figure adapted and translated from Figure 5.8 in Ref. [16]).

2.1.2. Met Mast

The 100 m met mast is located 1000 m east of the escarpment and is equipped with numerous measurement instruments, which are mounted at several heights. It is a met tower that meets the guidelines of the IEC 61400-12-1 (2005) standard for power performance measurements [22]. These include various first class cup anemometers (at 10 m, 25 m and 100 m), first class wind vanes (at 25 m, 50 m, 75 m and 92 m), barometers (at 5 m and 98 m), thermometers (at 5 m, 50 m, 75 m and 98 m), hygrometers (at 5 m, 50 m, 75 m and 98 m) and three three-dimensional (3-D) ultra sonic anemometers (*USA*) mounted at 50 m, 75 m and 98 m. In north-south direction the mast is equipped with booms of a length of 5 m to reduce the influence and the flow interaction with the met mast main body. The sampling frequency of the met mast sensors has been set to 20 Hz. In this context, first class means that the sensor has an accuracy class of 0.5 and meets all requirements of the IEC 61400-12-1 (2005) standard [22] for wind turbine power performance testing. The met mast therefore meets or exceeds wind industry best practices for wind measurements.
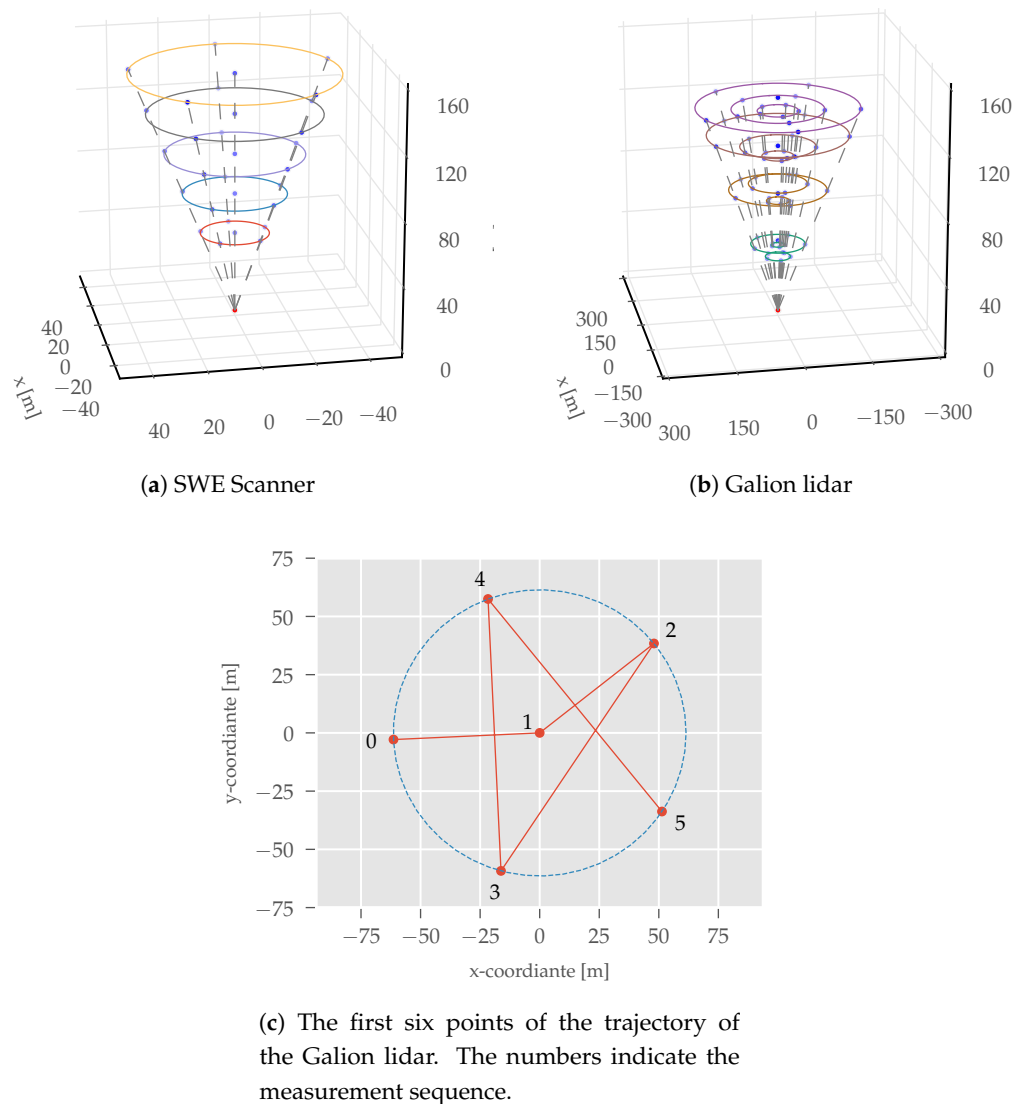
2.1.3. Lidar

The SWE Scanner system and Galion lidar were installed next to each other $\approx$300 m west of the met mast. Both lidar systems used pulsed lasers and so can measure several heights simultaneously.

The global coordinate system is a right hand system where the u or x_1-axis points in north direction, the v or x_2-axis points west direction and the w or x_3-axis points vertical to the sky. The wind direction corresponds to the Geographic Coordinates from north clock wise. The device coordinate systems ($\theta = 0°$) correspond to the global coordinate system (North).

The SWE Scanner was configured to use a modified VAD method known as the *six beam* trajectory [23]. The trajectory has five points on a circle with a half-opening angle of $\phi = 15°$ and one vertical point in the centre of the circle (Figure 4a). The azimuth angle θ is equally spaced on the circle with $\triangle\theta = 72°$. The scan duration of the trajectory was 8.8 s. Five focal distances were measured simultaneously (50 m, 75 m, 100 m, 125 m, 150 m) at each azimuthal position.

The Galion lidar has a maximum measurement range of approximately 4000 m. The device is fully configurable, with freely chosen azimuth and elevation angles and a maximum half opening angle of $\phi_{max} = 92°$. In this campaign, the device measured three *six beam* trajectories with three different opening angles $\phi_{1,2,3} = [20°, 39.2°, 55°]$ one after another (Figure 4b). These measurements were also used to test a method for determining the second statistical moments of the measured wind speed in complex terrain [24,25]. The opening angles used were therefore the same as used in [24]. The azimuth angle was equally spaced with $\triangle\theta = 72°$. The order of trajectory points was chosen to give the least time for every measurement sequence. The trajectory looks like a pentagram (Figure 4c) because the elevation angle can be changed faster than the azimuth angle. For a given combination of θ and ϕ the device is able to measure the radial velocity v_{los} at multiple focal distances df. The data

includes measurements for different distances ranging from 45 m to 735 m in 30 m intervals. The scan duration for all 18 points within the trajectory was 49 s.

(**a**) SWE Scanner　　　　　　　　　　　　　　　　(**b**) Galion lidar

(**c**) The first six points of the trajectory of the Galion lidar. The numbers indicate the measurement sequence.

Figure 4. Measurement trajectories for (**a**) the SWE Scanner and (**b**,**c**) the Galion lidar.

The two lidar systems differ in trajectory duration and in the configuration of the half opening angle ϕ. This difference in configuration enables the influence of these parameters on the measurement quality to be studied.

2.1.4. Data Filtering and Selection

In order to compare the different wind field reconstruction methods with the reference data from the met mast, these must be prepared and filtered in the pre-process. It is necessary to filter the data in order to accurately compare the different systems. The process of filtering and selection is shown in Figure 5. Data from the lidar and met mast are treated differently:

Lidar: The high-resolution recorded lidar data are processed with the wind field reconstruction methods: The last N data points are used for each time step. These methods determine both the wind velocity components u, v, w and statistical parameters (CNR_{mean}, CNR_{min} and CNR_{max}) for the carrier-to-noise ratio (CNR). The CNR parameters are still required for later data processing. The horizontal wind speed is calculated from the wind speed components u, v (Equation (2)).

These data are now subjected to a CNR filter to exclude samples outside of the CNR range. It is important that both the $CNR_{m}in$ and the CNR_{max} are within the CNR limits. Values outside these limits are not taken into account for further consideration. From these data the 10 min statistics are calculated and selected.

$$v_h = \sqrt{(u^2 + v^2)} \tag{2}$$

Met mast: The recorded data is first subjected to a plausibility test where the system checks that values are within a realistic range. If data is available from a second sensor at nearly the same height a comparison of the data from those sensors is also made, e.g., between the cup anemometer at 100 m and the horizontal wind speed from the sonic at 98 m. Then the 10 min statistics are calculated, and the data is selected according to the selection criteria in Table 1 .

The directional dependency of the lidar met mast data is checked in a different way, represented by the green path in Figure 5.
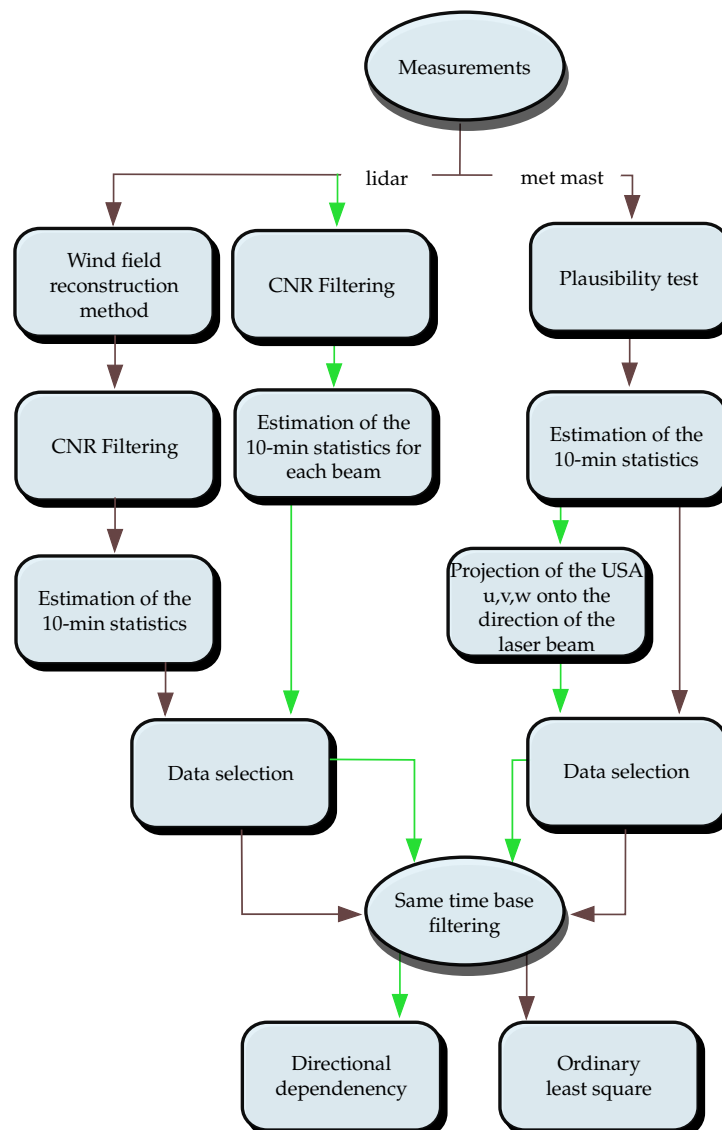

Figure 5. Steps in processing and selecting data from the lidar and met mast.

Table 1. Selection criterion used in Figure 5.

Parameter	Acceptable Range	
	Minimum	Maximum
Lidar measurements CNR (min, mean) [dB]	−22	10
Weather conditions Wind direction [°]	245	315
Temperature [°]	>2	-
Mast function Std. cup anemometer	>0.01	-
Data availability lidar [%]	90	100
met mast [%]	100	-

After filtering and selection, both data streams will contain gaps. Only lidar and met mast measurement data that are available at the same time step are used.

2.2. Wind Field Reconstruction Methods

Two different wind field reconstruction methods were used, the *Continuous least-square* method and a *linear* model, which additionally use the velocity gradient. In addition, these two algorithms are combined with predicted residual error sum of squares (*PRESS*) statistics.

$$\underbrace{\begin{bmatrix} v_{los1} \\ \vdots \\ v_{losN} \end{bmatrix}}_{\mathbf{b}} = \underbrace{\begin{bmatrix} n_{x1} & n_{y1} & n_{z1} \\ \vdots & \vdots & \vdots \\ n_{xN} & n_{yN} & n_{zN} \end{bmatrix}}_{\mathbf{A}} \underbrace{\begin{bmatrix} u \\ v \\ w \end{bmatrix}}_{\mathbf{x}} \tag{3}$$

2.2.1. Continuous Least-Square

This procedure, here referred to as continuous least-square (*CLS*), is a modified variant of the standard VAD method as used in commercial systems [26] to determine the wind velocity components. The idea behind this is that the velocity components are calculated continuously and not after just one trajectory cycle. This means that if the trajectory has N data points, the last N data points will be used for the calculation. Considering Equation (1), a system of equations (Equation (3)) can then be established from these N data points to determine the wind velocity components u, v, w from the lidar data. The matrix $\mathbf{A}$ of the equation system consists of the components of the normal vectors $\vec{n}(x, y, z)_i$ of the used N data points. To solve Equation (3), the vector $\mathbf{b}$ is multiplied by the inverse Matrix $\mathbf{A}^{-1}$. If the trajectory has more than three data points (which are at least necessary) the Moore-Penrose pseudoinverse $\mathbf{A}^{-1}$ will be used to solve the system of equations at the time step t. In order to solve this system of equations, it is not necessary to assume the homogeneous flow, since a solution is estimated which has the smallest absolute error. As a result, measurement errors (unrealistic data (e.g., due to bad CNR) strongly distort the solution of the equation system (Equation (3)). These unrealistic data must then be filtered in post-processing.

2.2.2. Predicted Residual Error Sum of Squares (PRESS)

The *PRESS* method [27,28] can be used to make the *CLS* procedure more robust. *PRESS* detects outliers and excludes them from the evaluation using leave-one-out cross validation. The *PRESS* method has been used for comparable applications such as cross-validation of samples [29], but this paper is the first known application of the *PRESS* method to lidar wind data.

In *PRESS*, the initial record—containing N data points—is reduced by one value and the reduced record N-1 is used to calculate the underlying model. The calculation scheme is represented in Figure 6 and repeats itself N times for each time step. The new estimated reconstructed line-of-sight velocity $\hat{v}_{los}$ are calculated from this solution and the inverted model. Then the coefficient of determination R^2 (Equation (4)) is calculated to quantify the goodness of fit. The R^2 is calculated as:

$$R^2 = \frac{SS_{reg}}{SS_{tot}} \tag{4}$$

$$SS_{reg} = \sum_i (\hat{v}_{los,i} - \overline{v}_{los})^2 \tag{5}$$

$$SS_{tot} = \sum_i (v_{los,i} - \overline{v}_{los})^2 \tag{6}$$

where SS is the sum of the squares for the regression ($_{reg}$) and the total ($_{tot}$); $\overline{v}_{los}$ represents the mean values and $\hat{v}_{los}$ is the reconstructed line-of-sight velocity. In each time step a different point is omitted. From these N iterations, the variant with the highest R^2 is selected for further post-processing.
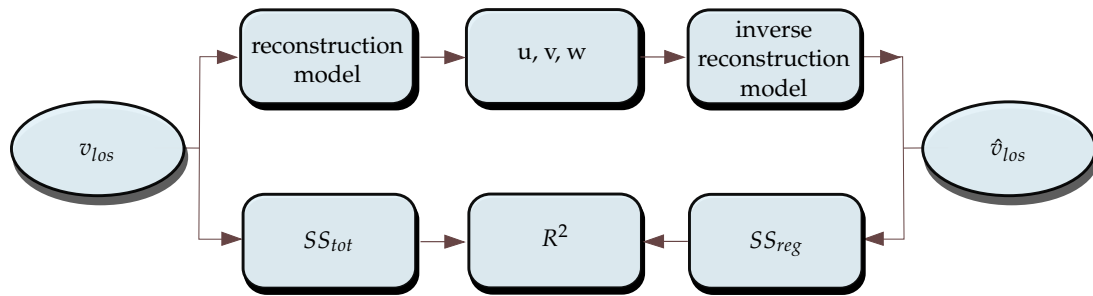
Figure 6. Overview of the workflow to estimate the combination of data points the maximized the coefficient of determination R^2, based on the input variables v_{los}, the estimated wind velocity components u, v, w, the model predicted $\hat{v}_{los}$ and the total sum of squares (SS_{tot}) and the regression sum of squares SS_{reg}.

2.2.3. Linear VAD Model

This procedure is based on the idea of converting the turbulent wind vector $\vec{v}(x, y, z)$ at the point x_0, y_0, z_0 into a linear function through a Taylor polynomial up to the first order to represent the inhomogeneous flow conditions in complex terrain more accurately. The resulting Taylor polynomial for the wind velocity vector $\vec{v}(x, y, z)$ is represented in Equation (7). This is made up of a stationary value $\vec{v}(x_0, y_0, z_0)$ and three directional derivative in space at the point of development (index 0).

$$\vec{v}(x,y,z) = \vec{v}(x_0,y_0,z_0) + \frac{\partial \vec{v}}{\partial x}(x - x_0) + \frac{\partial \vec{v}}{\partial y}(y - y_0) + \frac{\partial \vec{v}}{\partial z}(z - z_0) \tag{7}$$

$$\begin{aligned} v_{los} = {} & u_0 n_x + u_x' n_x (x - x_0) + u_y' n_x (y - y_0) + u_z' n_x (z - z_0) \\ & + v_0 n_y + v_x' n_y (x - x_0) + v_y' n_y (y - y_0) + v_z' n_y (z - z_0) \\ & + w_0 n_z + w_x' n_z (x - x_0) + w_y' n_z (y - y_0) + w_z' n_z (z - z_0) \end{aligned} \tag{8}$$

The linear approximation (Equation (8)) consists of twelve unknown variables. These are the three wind vector components (u, v, w with index 0) at the point x_0, y_0, z_0 and the other nine variables are the partial derivatives (mark with a *ı* in Equation (8)) of the three wind vector components in the Cartesian coordinate space (index x, y, z). This equation cannot be solved without further assumptions. Some terms have the same geometric identity and are linearly dependent: the components u_y' and v_x' and the terms u_z' and w_x' and the v_z' and w_y' terms had the same prefactors.

Each gradient pair has the same prefactors as shown in the example for u_y and v_x:

$n_x y = xy/f_d = xn_y$ with $n_x = x/f_d$ (f_d is the distance of the lidar measuring point).

To solve the Equation (8), two important assumptions have to be made:

1. The components are only evaluated along the vertical axis of the lidar device (coordinate origin), which means that $x_0 = y_0 = 0$.
2. The gradient of the vertical wind speed components in x- and y-direction w_x and w_y would be zero.

CFD simulations and the results show very small changes in the inclination angle at this test site that support the second assumption [16]. There are no more assumptions possible for the components u_y and v_x to simplify the Equation (8) and so the two terms are not separable. A case to simplify Equation (8) is when all trajectory points are located on a horizontal plane with the height $z_0 = z$, then the partial derivatives in the direction of z would disappear. In this work, a lidar system is used which works with constant focal lengths f_d and thus places the measuring points along a sphere in space.

With these assumptions it was possible to reduce the number of unknown variables from twelve to nine and a system of equations with these nine unknown variables is obtained. These nine variables consists of the three wind velocity components and the six simplified components of the strain tensor. In order to calculate the unknown components, at least nine linearly independent measuring points are required. The reduced system of equations is represented in Equation (9). On the left hand side is the known vector **b** which contains the N measured $v_{los\,i}$ and on the right hand side are the components of the normal vector in matrix **A** and the nine components of the linear approximation of the velocity vector in vector **x**. Equation (9) can be solved by inverting matrix $\mathbf{A}^{-1}$ and multiplying by the vector **b**.

$$
\underbrace{\begin{bmatrix} v_{los\,1} \\ \vdots \\ v_{los\,N} \end{bmatrix}}_{\mathbf{b}} = \underbrace{\begin{bmatrix} (n_x)_1 & (n_x x)_1 & (n_y)_1 & (n_y y)_1 & (n_z)_1 & (n_z z - z_0)_1 & (n_y x)_1 & (n_x(z-z_0))_1 & (n_y(z-z_0))_1 \\ \vdots & \vdots & \vdots & \vdots & \vdots & \vdots & \vdots & \vdots & \vdots \\ (n_x)_N & (n_x x)_N & (n_y)_N & (n_y y)_N & (n_z)_N & (n_z z - z_0)_N & (n_y x)_N & (n_x(z-z_0))_N & (n_y(z-z_0))_N \end{bmatrix}}_{\mathbf{A}} \underbrace{\begin{bmatrix} u_0 \\ \frac{\partial u}{\partial x} \\ v_0 \\ \frac{\partial v}{\partial y} \\ w_0 \\ \frac{\partial w}{\partial z} \\ \frac{\partial v}{\partial x} + \frac{\partial u}{\partial y} \\ \frac{\partial u}{\partial z} \\ \frac{\partial v}{\partial z} \end{bmatrix}}_{\mathbf{x}} \quad (9)
$$

3. Results

This section presents the results of the data analysis. First, the lidar data is compared with the three dimensional ultra sonic anemometers (*USA*) data to determine if there is a directional dependency. For this comparison, the 3-D velocity information from the *USA* are reduced to the line-of-sight velocity by applying a projection on to the direction of the laser beam. Furthermore, in a second step the results of the three wind field reconstruction methods are compared with the met mast data. For the comparison between lidar and met mast data the method of the ordinary least squares (OLS) is used. The data from the Galion lidar were used for further investigations. Furthermore, the influence of the opening angle on the correlation with the met mast was examined and whether the scan duration has an influence on the results. In order to compare the different methods with each other, the determined confidence intervals are compared with each other.

3.1. Directional Dependency

To find out if there is a directional dependency at this test site, the wind vector from the *USA* $\vec{v}_{usa}$ at 98 m was projected onto the normal vectors $\vec{n}_{lidar}$ of the laser beams of the SWE Scanner. The projection is done using Equation (1).

The relative and absolute differences depending on the wind direction and the horizontal wind speed for each azimuthal position of the laser beam are shown in Figure 7. When looking at these plots, it should be noted that the sector disturbed by turbine wakes is from 341° to 171° (Figure 1). Figure 7 clearly shows increases in differences between the lidar and ultrasonic measurements in this sector. A closer inspection of the beam in the 288° direction shows that the positive differences (red dots) are mainly in the direction of the escarpment. There also appears to be an effect of the flow direction on the sign of the difference between the projected lidar wind speed and the value from the met mast in some sectors, whereby flow towards the lidar has a positive difference and flow away has a negative difference. This effect can be seen clearly in the beams at 288° and 216° but less so in the other directions. The particularly small differences do not appear to depend on direction or wind speed and also appear to have random distribution.

When the wind is perpendicular to the laser direction (e.g., from 18° or 198° for the azimuthal beam from 288°), the lidar can only observe the existing vertical component w and the horizontal components should be zero if the alignment is perfect. This arises from Equation (3). From Figure 7 it can be seen that the points on the axes orthogonal to the beam do not have zero magnitude. However, because of different sampling rates, the chance that the lidar and met mast were not perfectly aligned (despite using best practice), and the possibility that the wind direction was not exactly the same at the lidar and mast, it is impossible to say that this difference is solely the vertical wind component w.
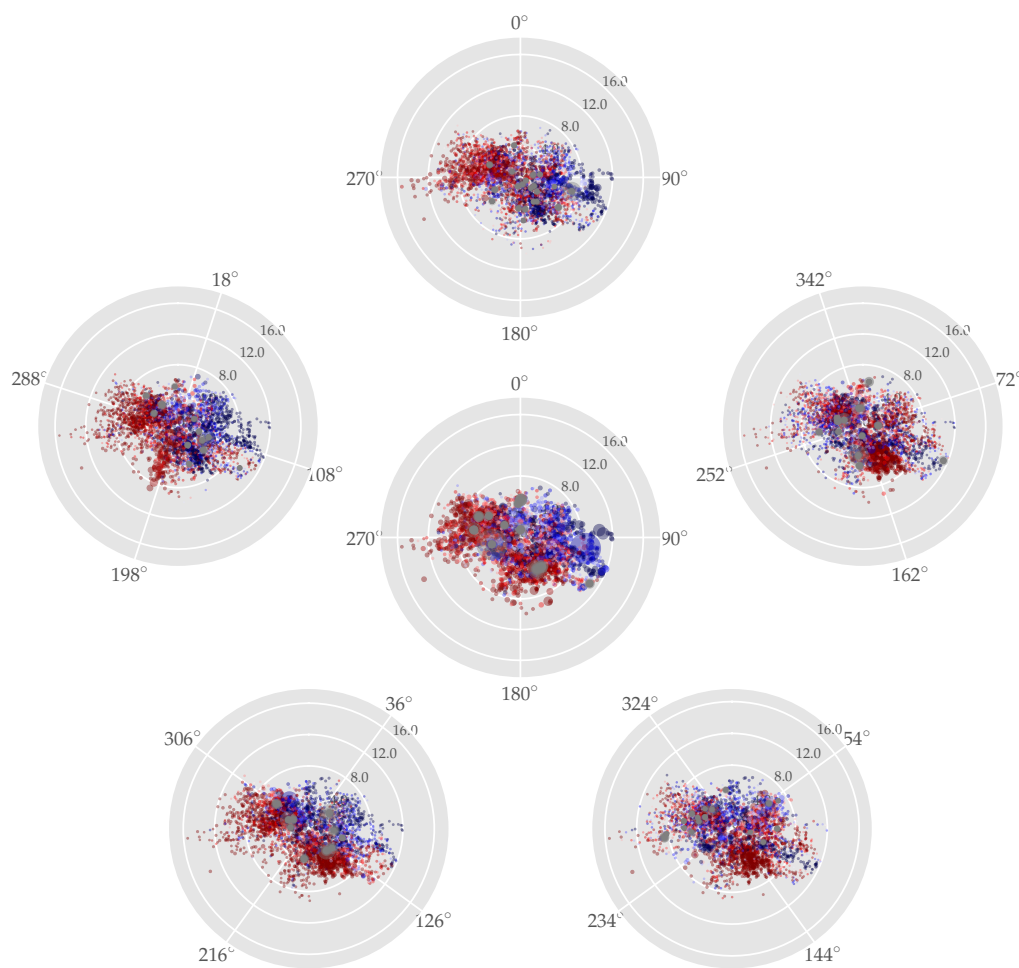
Figure 7. Results of the projection of the *USA* onto the five lidar beam normal vectors. Each polar plot represents a combination of azimuth-elevation angles of the laser beam. The positions of the plots correspond to the azimuth angle of the scanner laser beam: the upper left graph is equivalent to the azimuth angle at 288°, the lower left graph is equivalent to 216°, the middle graphic is the vertical measurement, etc. The axes of the graphs are rotated in the respective angles of the laser beam direction. The azimuth is the wind direction from the met mast. The distance of the point from the origin corresponds to horizontal wind speed (8, 12, 16mper s). The absolute differences between met mast and lidar ($\vec{v}_{usa} \cdot \vec{n}, i_{lidar} - \overline{v}_{los,i}$) are represented in colour and the size of points shows the relative differences between met mast and lidar. Positive absolute differences are marked in red, very small differences (magnitude < 0.001) are shown in grey, and negative differences in blue.
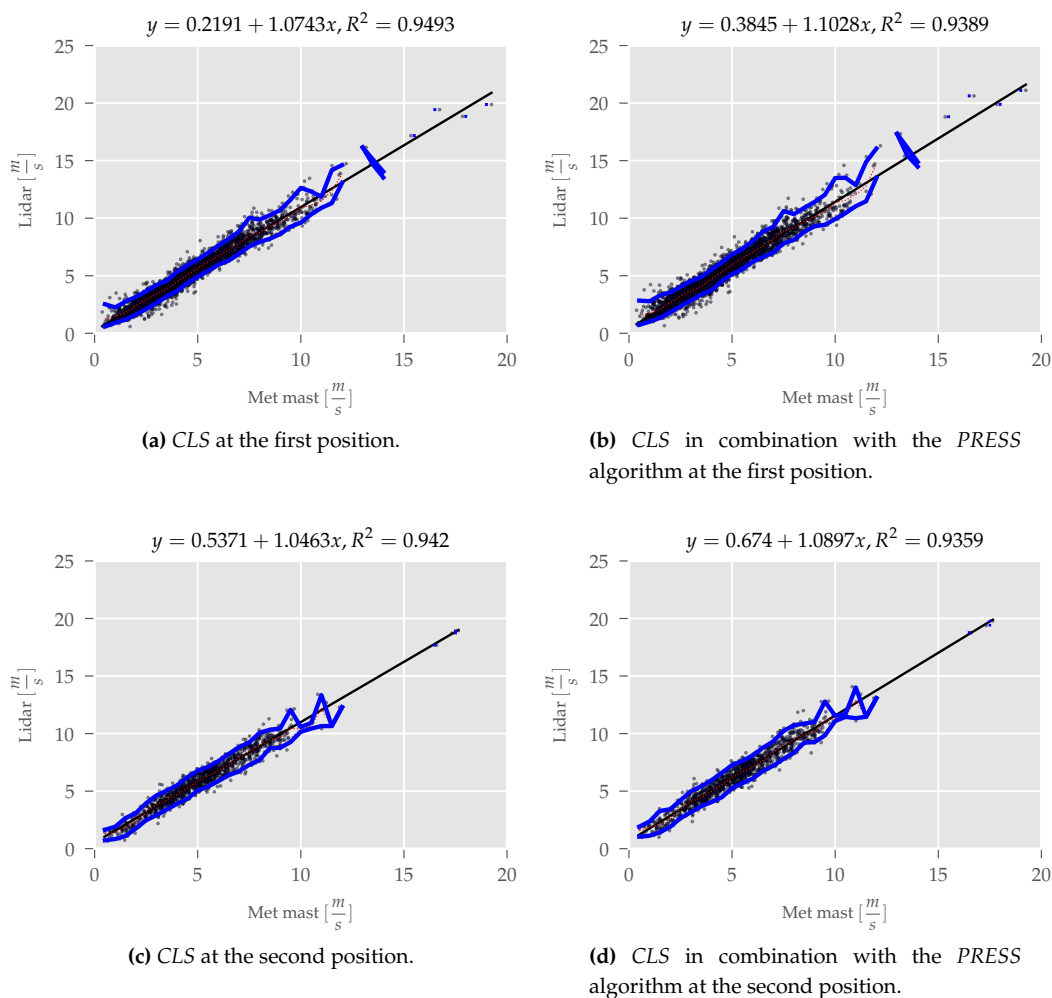
3.2. Wind Speed Comparisons

In this subsection the results of the different wind field reconstruction method compared to the cup anemometer are presented. The results of the statistical parameters of the OLS are summarized in Table 2.

SWE Scanner: Figure 8 shows the results of the comparison between the SWE Scanner and the cup anemometer installed at 100 m using the *CLS* and *PRESS* methods.

The results show very similar results for the methods and locations which are investigated. The parameter offset differs by up to 0.4 m·s^{-1} between the results and the slope changes by 0.04 between the lowest and the highest value. R^2 is similar with values between 0.94 and 0.95. It is noticeable that the results with *PRESS* (Figure 8b,d) have larger offsets and slopes than the *CLS* method (Figure 8a,c). These 10 min lidar data contain the point combinations that had the highest R^2 in time

step *t*, which should reduce the effect of outliers. However, this does not lead to an improvement in the agreement between lidar and mast.

The investigated wind speed range in this case was range 0–20 m·s^{-1}. Data are most frequent in the lower range (up to 10 m·s^{-1}), where the 5–95th quantile range of the data is large compared to that seen in the more sporadic wind speeds over 15 m·s^{-1}.

(a) *CLS* at the first position.

(b) *CLS* in combination with the *PRESS* algorithm at the first position.

(c) *CLS* at the second position.

**(d)** *CLS* in combination with the *PRESS* algorithm at the second position.

Figure 8. Correlation between SWE Scanner and the cup anemometer at 100 m above ground. The black dots represent the 10 min data points, the black line is the regression line, and the blue lines are the 5th and 95th quantiles.

The same comparison was also made using data from the SWE scanner at the second measurement location near the foot of the met mast. For brevity these results are not shown here. Results at this second (closer) site deviate more from the met mast at low wind speeds than at the first (further) site. At speeds greater than 8.8 m·s^{-1}, the deviations are smaller compared to position one. These results suggest that the improvement in agreement between the lidar and the met mast are due to the measurement method, not the different locations.

Galion: The results from the Galion system are shown in Figure 9. For the *CLS* method all 18 trajectory points were used for the evaluation. A multiple overdetermined system of equations has to be solved. This lidar and method shows a better agreement between the lidar measurements and the met mast than the SWE Scanner measurements (Figure 9a; offset 0.018 m·s^{-1}, slope 1.033, R^2 0.974).

(a) All points

(b) $\phi = 20°$

(c) $\phi = 39.2°$

(d) $\phi = 55°$

(e) *linear* flow model
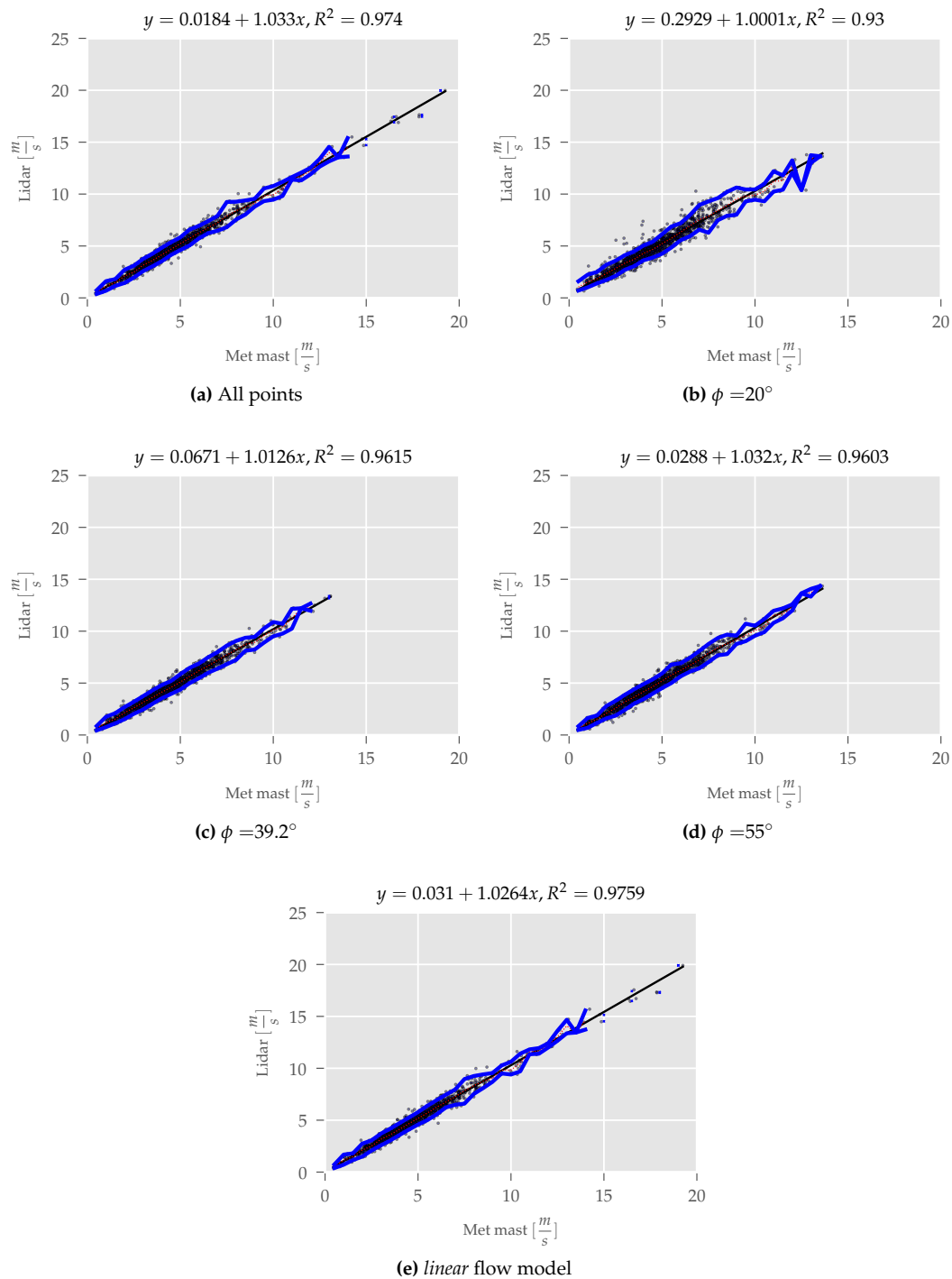
Figure 9. Correlation between Galion lidar and the cup anemometer at 100 m above ground. The black dots represent the 10 min data points, the black line is the regression line, and the blue lines are the 5th and 95th quantiles.

The trajectory of the Galion lidar consists of three identical trajectories with different half opening angles ϕ. In order to check whether there is an influence of the opening angle on the measuring quality, the three trajectories were examined and evaluated separately (Figure 9b–d). It can be seen that reducing the opening angle—implying a sharper cone which is narrower at a given height—leads to a worse correlation (i.e., increased offset, slope further from 1.0, or reduced R^2; details are in the Figures).

Results from the *linear* model are presented in Figure 9e. The offset is 0.03 and the slope (1.026) implies results that are very close to the met mast measurements. The dispersion of the data is small
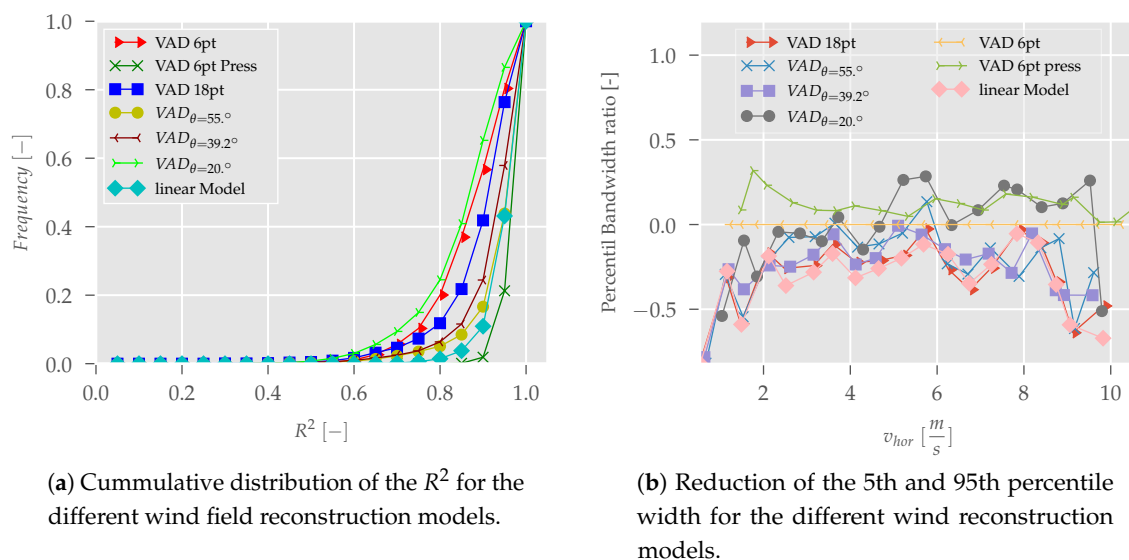
($R^2 = 0.976$), the width of the 5–95th quantile is significantly reduced. Increased relative errors occur in the lower wind speed range (≤ 2 m·s^{-1}), likely due to the high turbulence intensity that reduces homogeneity across the measurement cone. However, this wind speed range is not relevant for the production of wind energy.

Table 2. Summary of the OLS (Ordinary least-squares) results.

Lidar System	Method	Slope [-]	Offset [m·s^{-1}]	R^2
SWE Scanner	*CLS*	1.074	0.219	0.949
SWE Scanner	*PRESS*	1.103	0.385	0.938
SWE Scanner 2nd position	*CLS*	1.046	0.537	0.942
SWE Scanner 2nd position	*PRESS*	1.09	0.674	0.936
Galion 18 Pts.	*CLS*	1.033	0.02	0.974
Galion 20°	*CLS*	1.00	0.293	0.93
Galion 39.2°	*CLS*	1.013	0.067	0.962
Galion 55°	*CLS*	1.032	0.03	0.960
Galion	*linear*	1.026	0.03	0.976

3.3. Comparison of the Statistical Parameters of Methods

Figure 10a shows the cumulative relative occurrence of R^2 of individual 10 min data for the different methods. The *PRESS* method has a very concentrated distribution with all R^2 greater than 0.85, and over 78% of the R^2 data greater than 0.95. The *CLS* method in combination with the SWE Scanner has the widest distribution of the systems and methods that was investigated. The results when using the Galion with an opening angle of $\phi = 20°$ are similarly wide, the differences of the shape of the distribution is very similar to the distribution of the SWE Scanner.

(**a**) Cummulative distribution of the R^2 for the different wind field reconstruction models.

(**b**) Reduction of the 5th and 95th percentile width for the different wind reconstruction models.

**Figure 10.** Overview of the distribution of R^2 and the reduction of the 5th and 95th percentile.

A comparison of the ranges of quantiles for the individual methods against a reference value gives a good impression of the relative dispersion of the individual methods. For this purpose the width of the 5–95th quantile is calculated for each method (Figure 10b). The results of the SWE Scanner with the *CLS* method were taken as reference because this trajectory is very similar to commercial lidar wind profilers. The narrowest quantile is observed using the *linear* model and the *CLS* model for the Galion Lidar with all 18 trajectory points. These procedures achieve a reduction between 20% and 60%.

In comparison, the *PRESS* method raises the dispersion by up to 20%. The range is reduced for the other procedures, but not in order as for the *linear* model.

4. Discussion

The projection of the met mast *USA* data onto the normal vector of the lidar showed a directional dependence. This is in line with observations that the terrain significantly influences the inflow over the *Albtrauf* [16,21]. CFD analysis [16] does not give a value to quantify the difference and, the CFD analysis assumes neutral stratification. If stratification effects are added as in reality, this could explain the discrepancies between the lidar and the *USA*.

The difference in error between the met mast and wind field reconstruction using the *CLS* and *PRESS* methods is shown in Figure 11. The results are visualized using the frequency of $|v_{cup} - v_{CLS}| - |v_{cup} - v_{PRESS}|$. Consider a case where the reference or 'true' wind speed is 10 m·s^{-1}, and the *CLS* result is 9.7 m·s^{-1} while the *PRESS* result is 10.2 m·s^{-1}. In this case, the *PRESS* method has led to a better wind field reconstruction, and the result is 0.3 m·s^{-1} − 0.2 m·s^{-1} = 0.1 m·s^{-1}. In this study of 3820 data points, the *CLS* method resulted in a lower error in 91.1% of the measurement periods. One reason for this is, that the additional measuring point of the *CLS* method reduces the reconstruction error compared to the *PRESS* algorithm; the reconstruction error for the wind components is proportional to $1/\sqrt{N}$ where N as number of laser beams [30]. This is also surprising as it was hoped initially that the *PRESS* method would be more robust than the *CLS* method because of the rejection of outliers.
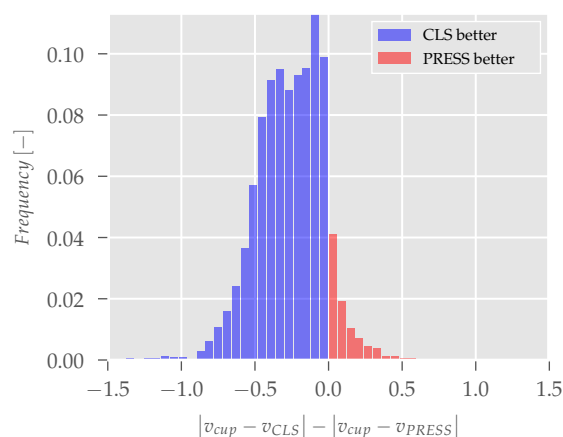
Figure 11. The error in the wind field reconstruction using the *CLS* method, versus the error due to the *PRESS* method. Negative values indicate that the *CLS* method had lower error compared to the met mast than the *PRESS* for a particular 10-minute period.

In the previous section, the correlation between the presented methods applied to lidar measurements and the horizontal wind speeds of in-situ sensors mounted on a met mast was presented. From those results it can be observed that a suitable measurement strategy can improve the agreement between the lidar and met mast.

In this study, using the *linear* model the agreement with the met mast was considerably improved. The results varies in the magnitude of the CFD simulation of ≈2% and the offset is nearly zero with 0.03 m·s^{-1}.

In addition, the width of the 5–95th quantile is significantly reduced in average of 26.96%. In summary, it is a clear improvement using the *linear* method compared to the *CLS* method. Due to the extended *linear* model, the horizontal wind speed in complex flow (at least at this location) can be determined much more precisely than with the standard VAD method. Whether this model delivers useful results in general for complex locations is still to be verified by further tests. For this location,

the correlation is closer to unity and the offset is nearly zero. Furthermore, there are also optimization possibilities for this model in the trajectory configuration as well as in the selection of the angles ϕ and θ.

If this result is related to the distributions of R^2 (Figure 10a), then the influence of the used model is clearly visible. For the *PRESS* method, the R^2 distribution shows a very concentrated form with over 75% of the data with over $R^2 \geq 0.95$. The results of the correlation (Figure 8b) show, however, the worst matches with the measuring mast data. This has the highest offset, the highest slope and the smallest R^2, as well as the widest confidence interval. The results in Figure 10a shows a very good agreement between the data and the used model, however Figure 8b shows that the used model does not match the met mast measurements.

These results show that increasing the half opening angle ϕ leads to better correlations between the lidar and mast. The reason for this is that the deterministic error is reduced. This aspect has been shown by the determination of the second statistical moment by lidar data using an analytical model [23]. The optimum angle of a four point VAD method was estimated with an analytical solution to $\phi = 54.7356°$ [30]. This correlates very well with the result in this study. The condition number κ of the **A** solution matrix illustrates this. The κ describes the sensitivity of the solution to changes in the data. This means that in worst case, the input error is amplified by this κ.

The condition number κ of the different solutions tested here is shown in Table 3. The largest κ occurs in the *CLS* procedure for the SWE Scanner with a $\phi = 15°$. The smallest κ is found using the *CLS* method with a $\phi = 55°$. The ratio between largest and smallest κ (4.6) is not directly reflected in difference between the results, but the ability of κ to identify improved scan geometry for the same analysis methods is confirmed by the results.

The question that naturally arises is, how representative are measurements with a $\phi = 55°$ at a measuring height of 100 m? After all, the radius of the circle for this configuration is 76.5 m. This question cannot be answered without further investigation. For load simulations of wind turbines according to IEC 61400-01 [31], coherent wind fields are created using the exponential coherence model. This model depends on the average wind speed, distance of the observed points and the considered frequency. The validity of the coherence model is related to structures in the wind fields and the wind evolution over time and space, and should be investigated in future studies.

Table 3. Characteristics for the different configurations.

	SWE Scanner			Galion			
	VAD 5+1	VAD 18	ϕ_{20}	$\phi_{39.2}$	ϕ_{55}	*linear*	
ϕ [°]	15	15	20, 39.2, 55	20	39.2	55	20, 39.2, 55
scan duration [m·s^{-1}]	8.8	4.78	49	16.3	16.3	16.3	49
κ [-]	5.78	5.78	2.02	4.30	2.00	1.26	120.66
Nb. of Points [-]	6	6	18	6	6	6	18
Location [-]	1	2	1	1	1	1	1

Another aspect that needs to be addressed here is the influence of the different scan durations on the measurement results. An overview of the detailed scan duration for the different trajectories is listed in Table 3. The SWE Scanner measures 5.57 times more data in 10 min than the Galion. This should lead to a reduction of the random error. This can be seen to a lesser extent in the comparison of Figures 8a and 9b which measured with a very similar ϕ. The characteristic of the different trajectories are listed in Table 3. The differences between these two half opening angles are marginal (the offset differs by 0.074 m·s^{-1}, the slope by 0.074 and R^2 by 0.019). At the second position the scan duration was reduced by a factor of 1.84, but there are no noticeable improvements. The averaged error over the wind speed range between 0 m·s^{-1} and 20 m·s^{-1} is for *CLS* at the first position 1.034 m·s^{-1} and at the second position is a bit less with 1.00 m·s^{-1}. Unfortunately, the question of the influence of the scan duration cannot be answered on the basis of the results. It is quite clear that the random error is reduced by a higher data availability, but other effects (e.g., opening angle) have a greater influence. Conducting

additional experiments in flat terrain with homogeneous flow conditions would be a possible solution there to answer the question on the scan duration.

Further investigations are also necessary into the suitability of the *linear* model. It should be used at more sites to see if the results observed here apply for different complex terrains types. Furthermore, the gradients should be examined to see whether the assumed values are plausible and realistic. This could be done with the help of CFD simulations, or with the help of gradients the numerical simulation can be validated more precisely. So far, only the 10 min statistics have been compared; investigations with high-resolution data and in the frequency domain should also be carried out.

5. Conclusions

In this study, different methods for lidar-based wind field reconstruction in complex terrain were investigated. The main objective was to reduce uncertainties in the measurements by using optimized methods for wind field reconstruction. As a side product, the influence of the opening angle and the scanning duration could also be investigated. Two different methods were investigated and these were additionally coupled with the statistical *PRESS* procedure. The result of the *CLS* method in combination with *PRESS* shows a very skewed distribution of high values of R^2 based on the 10 min data, but this is not reflected in the correlation comparison with the in-situ measurements at the met mast. The results of the correlation are worse than the results of the *CLS* method without *PRESS* statistics. It could be shown that with the *linear* model for wind field reconstruction the agreement with the measurements of the in-situ sensors can reach the level of measurements with homogeneous flow. Furthermore, the range of the 5–95th quantile could be reduced by 32.2% on average compared to the reference VAD method. Furthermore, the influence of the opening angle on the measurement results could be shown. The agreement with the mast measurements and the width of the 5–95th quantile was reduced with larger half opening angles ϕ. The influence of the scan duration on the uncertainties reduction could not be verified with the current data set and measurement set up. In future measurement campaigns with complex flow, the *linear* model with an optimized trajectory should be used. However, this naturally also requires an appropriate lidar system in which the azimuth and elevation angle can be adjusted because for the application of the *linear* model, three different half-opening angles ϕ are necessary. This is currently not possible with the standard lidar wind profilers and it requires so-called all sky scanning devices.

References

1. Weitkamp, C. *Lidar: Range-Resolved Optical Remote Sensing of the Atmosphere*; Springer Science+Business Media Inc.: New York, NY, USA, 2005.
2. Clifton, A.; Clive, P.; Gottschall, J.; Schlipf, D.; Simley, E.; Simmons, L.; Stein, D.; Trabucchi, D.; Vasiljevic, N.; Würth, I. IEA Wind Task 32: Wind Lidar Identifying and Mitigating Barriers to the Adoption of Wind Lidar. *Remote Sens.* **2018**, *10*, 406. [CrossRef]
3. Courtney, M.; Wagner, R.; Lindelöw, P. Testing and comparison of lidars for profile and turbulence measurements in wind energy. *IOP Conf. Ser. Earth Environ. Sci.* **2008**, *1*, 012021. [CrossRef]

4. Alberts, A.; Janssen, A.; Mander, J. German Test Station for Remote Wind Sensing Devices. EWEC, Marseille, 2009. Available online: https://www.researchgate.net/profile/Axel_Albers/publication/237616810_German_Test_Station_for_Remote_Wind_Sensing_Devices/links/568e2aee08ae78cc0514b121.pdf (accessed on 10 September 2018).

5. Clifton, A.; Boquet, M.; Burin Des Roziers, E.; Westerhellweg, A.; Hofsäß, M.; Klaas, T.; Vogstad, K.; Clive, P.; Harris, M.; Wylie, S.; et al. *Remote Sensing of Complex Flows by Doppler Wind Lidar: Issues and Preliminary Recommendations*; Technical Report; NREL (National Renewable Energy Laboratory (NREL): Golden, CO, USA, 2015.

6. Clive, P.J.M. Compensation of bias in Lidar wind resource assessment. *Wind Eng.* **2008**, *32*, 415–432. [CrossRef]

7. Bingöl, F.; Mann, J.; Foussekis, D. Conically scanning lidar error in complex terrain. *Meteorol. Z.* **2009**, *18*, 189–195. [CrossRef]

8. Mikkelsen, T.; Mann, J.; Courtney, M.; Sjöholm, M. Windscanner: 3-D wind and turbulence measurements from three steerable doppler lidars. *IOP Conf. Ser. Earth Environ. Sci.* **2008**, *1*, 012018. [CrossRef]

9. Pauscher, L.; Vasiljevic, N.; Callies, D.; Lea, G.; Mann, J.; Klaas, T.; Hieronimus, J.; Gottschall, J.; Schwesig, A.; Kühn, M.; et al. An Inter-Comparison Study of Multi- and DBS Lidar Measurements in Complex Terrain. *Remote Sens.* **2016**, *8*, 782. [CrossRef]

10. Vasiljević, N.; Palma, J.M.; Angelou, N.; Carlos Matos, J.; Menke, R.; Lea, G.; Mann, J.; Courtney, M.; Frölen Ribeiro, L.; Gomes, V.M. Perdigão 2015: Methodology for atmospheric multi-Doppler lidar experiments. *Atmos. Meas. Tech.* **2017**, *10*, 3463–3483. [CrossRef]

11. Mann, J.; Angelou, N.; Arnqvist, J.; Callies, D.; Cantero, E.; Arroyo, R.C.; Courtney, M.; Cuxart, J.; Dellwik, E.; Gottschall, J.; et al. Complex terrain experiments in the New European Wind Atlas. *Philos. Trans. R. Soc. A Math. Phys. Eng. Sci.* **2017**, *375*, 20160101. [CrossRef] [PubMed]

12. Schlipf, D.; Rettenmeier, A.; Haizmann, F.; Hofsäß, M.; Courtney, M.; Cheng, P.W. Model based wind vector field reconstruction from lidar data. In Proceedings of the 11th German Wind Energy Conference DEWEK 2012, Bremen, Germany, 7–8 November 2012. [CrossRef]

13. Bradley, S.; Strehz, A.; Emeis, S. Remote sensing winds in complex terrain—A review. *Meteorol. Z.* **2015**, *24*, 547–555. [CrossRef]

14. Klaas, T.; Pauscher, L.; Callies, D. LiDAR-mast deviations in complex terrain and their simulation using CFD. *Meteorol. Z.* **2015**, *24*, 591–603. [CrossRef]

15. Schulz, C.; Hofsäß, M.; Anger, J.; Rautenberg, A.; Lutz, T.; Cheng, P.W.; Bange, J. Comparison of Different Measurement Techniques and a CFD Simulation in Complex Terrain. *J. Phys. Conf. Ser.* **2016**, *753*, 082017. [CrossRef]

16. Schulz, C. Numerische Untersuchung des Verhaltens von Windenergieanlagen in Komplexem Gelände unter Turbulenter AtmosphäRischer Zuströmung. Ph.D Thesis, Universität Stuttgart, Stuttgart, Germany, 2018.

17. Rettenmeier, A.; Bischoff, O.; Hofsäß, M.; Schlipf, D.; Trujillo, J. Wind Field Analysis Using A Nacelle-Based LiDAR System. In Proceedings of the EWEC, Warsaw, Poland, 20–23 April 2010.

18. Wildmann, N.; Bernard, S.; Bange, J. Measuring the local wind field at an escarpment using small remotely-piloted aircraft. *Renew. Energy* **2017**, *103*, 613–619. [CrossRef]

19. Schulz, C.; Klein, L.; Weihing, P.; Lutz, T. Investigations into the Interaction of a Wind Turbine with Atmospheric Turbulence in Complex Terrain. *J. Phys. Conf. Ser.* **2016**, *753*, 032016. [CrossRef]

20. Hofsäß, M.; Bergmann, D.; Bischoff, O.; Denzel, J.; Cheng, P.W.; Lutz, T.; Peters, B.; Schulz, C. *Lidar Complex*; Technical Report; Universität Stuttgart, Fakultät 6 Luft- und Raumfahrttechnik und Geodäsie, Institut für Flugzeugbau (IFB), Stuttgarter Lehrstuhl für Windenergie: Stuttgart, Germany, 2017. [CrossRef]

21. Anger, J.; Bange, J.; Blick, C.; Brosz, F.; Emeis, S.; Fallmann, J. *Erstellung einer Konzeption eines Windenergie-Testgeländes in bergig komplexem Terrain : Kurztitel: KonTest : Abschlussbericht des Forschungsprojektes: ein Vorhaben des WindForS Windenergie Forschungscluster Forschungsnetzwerks*; Technical Report; Universität Stuttgart–Stuttgarter Lehrstuhl für Windenergie (SWE) am Institut für Flugzeugbau (IFB): Stuttgart, Germany, 2015. [CrossRef]

22. IEC (International Electrotechnical Commission). *Wind Turbines. Part 12-1, Power Performance Measurements of Electricity Producing Wind Turbines*; Number 12, 1; IEC: Geneva, Switzerland, 2005.

23. Sathe, A.; Mann, J.; Vasiljevic, N.; Lea, G. A six-beam method to measure turbulence statistics using ground-based wind lidars. *Atmos. Meas. Tech.* **2015**, *8*, 729–740. [CrossRef]

24. Frisch, A.S. On the measurement of second moments of turbulent wind velocity with a single Doppler radar over non-homogeneous terrain. *Bound.-Layer Meteorol.* **1991**, *54*, 29–39. [CrossRef]

25. Hofsäß, M.; Bischoff, O.; Cheng, P.W. Comparison of second moments between remote sensing devices in complex errain. In Proceedings of the 18th International Symposium for the Advancement of Boundary-Layer Remote Sensing, Varna, Bulgaria, 6–9 June 2016.

26. Peña, A.; Hasager, C.B.; Badger, M.; Barthelmie, R.J.; Bingöl, F.; Cariou, J.P.; Emeis, S.; Frandsen, S.T.; Harris, M.; Karagali, I.; et al. *Remote Sensing for Wind Energy*; DTU Wind Energy: Roskilde, Denmark, 2015.

27. Allen, D.M. Mean Square Error of Prediction as a Criterion for Selecting Variables. *Technometrics* **1971**, *13*, 469–475. [CrossRef]

28. Allen, D.M. The Relationship Between Variable Selection and Data Agumentation and a Method for Prediction. *Technometrics* **1974**, *16*, 125–127. [CrossRef]

29. Draper, N.R.; Smith, H. *Applied Regression Analysis*, 3rd ed ed.; Wiley Series In Probability and Statistics; Wiley: New York, NY, USA, 1998.

30. Teschke, G.; Lehmann, V. Mean wind vector estimation using the velocity–azimuth display (VAD) method: An explicit algebraic solution. *Atmos. Meas. Tech.* **2017**, *10*, 3265–3271. [CrossRef]

31. IEC (International Electrotechnical Commission). *Wind turbines. Part 1, Design Requirements*; IEC: Geneva, Switzerland, 2014.